Electron temperature profile collapse induced by double-odd-parity MHD mode in the Large Helical Device

Electron temperature profile collapse induced by double-odd-parity MHD mode in Large Helical Device

T. Kobayashi[1,2]**, K. Ida**[1]**, Y. Suzuki**[1,2]**, H. Takahashi**[1,2]**, Y. Takemura**[1]**,**

M. Yoshinuma[1]**, H. Tsuchiya**[1]**, M. Sanders**[3]**, and LHD Experiment**

Group

[1] National Institute for Fusion Science, National Institutes of Natural Sciences, Toki 509-5292, Japan

[2] SOKENDAI (The Graduate University for Advanced Studies), Toki 509-5292, Japan

[3] Eindhoven University of Technology, Eindhoven, 5600 MB, Netherlands

E-mail: `kobayashi.tatsuya@nifs.ac.jp`

Abstract. In this paper, we report new results of a beam switching experiment aiming at a reversed magnetic shear profile formation for the study of an MHD mode induced profile collapse event. A transient MHD mode whose oscillation frequency chirps down is observed. The electron temperature profile collapse is induced by the mode activity, leading to the flattening of the central electron temperature profile. The radial mode structure is the double-odd-parity at the beginning, but it transits to the even-parity in its final stage. The central electron temperature profile recovers after the radial mode structure changes to the even-parity, even though the mode itself does not disappear.

1. Introduction

In order to produce a sufficiently high temperature plasma in fusion devices toward the reactor, it is crucially essential to understand the physics of the plasma profile formation. One of the key elements is how the rotational transform ι, $2\pi/\iota = q$ where q is the safety factor, impacts on the electron temperature profile formation. There have been a number of investigations related to this issue, e.g., the relation between the low order rational surface and the internal transport barrier location [1, 2, 3], the transport barrier enhancement by the electron cyclotron current drive (ECCD) [4, 5] or the lower hybrid current drive (LHCD) [6], and the profile collapse induced by MHD modes [7, 8, 9, 10, 11] including disruptions [12]. In particular, transient global MHD activities often limit the plasma performance by terminating the profile growth or leading to disruptions. Therefore, much attention is paid to avoid these MHD events by various active control techniques [13].

In heliotron devices such as the Large Helical Device (LHD), there are generally no disruptions, therefore investigations for the profile collapse events induced by the transient MHD modes can be safely performed. In LHD, the rotational transform profile at the core can be varied by the plasma current induced by the tangentially injected neutral beam (NB) or the electron cyclotron current drive (ECCD). In particular, the beam switching from the co-beam to the counter-beam enhances flattening of the rotational transform profile and even produces a reversed shear profile [14, 15]. This operation was used for studying the static island formation in LHD, and it was revealed

that the island property was highly sensitive to the local magnetic shear [16]. The MHD mode activity when the magnetic shear is weakened or the reversed shear profile is formed under the beam switching operation is the next topic of interest.

In this paper, we report new results of a beam switching experiment aiming at a reversed magnetic shear profile formation for the study of an MHD mode induced profile collapse event. A transient MHD mode whose oscillation frequency chirps down is observed. The electron temperature profile collapse is induced by the mode activity, leading to the flattening of the central electron temperature profile. The radial mode structure is the double-odd-parity at the beginning, but it transits to the even-parity in its final stage. The central electron temperature profile recovers after the radial mode structure changes to the even-parity, even though the mode itself does not disappear. The present observations contribute to the literature by exemplifying a profile collapse event induced by a peculiar MHD mode in the stellarator devices.

2. Experimental results

2.1. Time evolution of the electron ITB collapse event

The experiments were conducted in the Large Helical Device (LHD). The magnetic axis in the vacuum configuration is set to $R_{\mathrm{ax}} = 3.6$ m, the so-called inward shifted configuration, with the toroidal field of $B_{\mathrm{t}} = 2.75$ T directed clockwise when viewed from the torus top. The plasma minor radius is defined by the averaged minor radius in which 99 % of the plasma kinetic energy is confined, to be $a_{99} \sim 0.6$ m. In the

vacuum configuration, the rotational transform profile $\iota/2\pi$ typically has a 1/2 rational surface in the mid-minor radius of $r_{\text{eff}} \sim 0.3$ m, where r_{eff} indicates the effective minor radius [17], and monotonically increases towards the edge. Although the confinement magnetic field is mainly generated by the external helical coils, various plasma current components including the currents driven by the neutral beam injection (NBI) and the electron cyclotron current drive (ECCD) alter the vacuum rotational transform profile. In particular, by performing the beam switching operation from the co-directed NBI to the counter-directed NBI, flattening or reversal of the rotational transform profile is observed [14, 15]. Here, the co-direction corresponds to the direction of the toroidal magnetic field and hence the direction of the equivalent plasma current in LHD. Therefore, a stationary co-directed plasma current increases the rotational transform from its vacuum value. Figure 1 shows the time evolution of the target discharge. At $t = 5.5$ s, the NBI is switched from the co- to counter-direction, which overturns the direction of the total plasma current drive. The abrupt change of the off-axis NB driven counter-directed current excites the co-directed current in the core region that decelerates the total plasma current change slower than the resistive time scale. This co-current at the core leads to the increase of the rotational transform value at the core and therefore enhances the flattening or reversal of the rotational transform profile. Before the beam switching, the two co-ECCDs focused in the plasma core region are applied both to realize the peaked electron temperature profile and to drive the co-directed plasma current at the core. The line averaged density is kept approximately constant at

slightly below 1×10^{19} m^{-3}. Note that the double-odd-parity mode discussed below is

not observed in the discharges in which the line averaged density exceeds 1.5×10^{19} m^{-3}.

The electron temperature profile drastically evolves in time after the beam switching

as shown in Fig. 1 (c). A gradual reduction of the central electron temperature starts

approximately one hundred milliseconds after the beam switching, and continues until

$t \sim 5.81$ s, in which a sharp collapse of the central electron temperature occurs.

Immediately after the collapse, the central electron temperature turns to recover, and

peaked electron temperature profile is regenerated at $t \sim 5.92$ s. Time evolutions of

the electron density profile, the electron temperature profile, and the ion temperature

profile are shown in Figs. 1 (d)-(f). The profile flattening is seen not only in the

electron temperature profile but also in the ion temperature profile, although it is rather

ambiguous. The profile collapse does not occur in the electron density profile since it

is almost flat in the core region. According to the saddle loop magnetic coil array

measurement, the static magnetic island dynamics is not responsible for the electron

temperature profile collapse, unlike the case in Ref. [10, 11].

2.2. Double-odd-parity MHD mode that induces electron temperature profile collapse

The temperature profile collapse is considered to be induced by a MHD mode activity.

Figure 2 (a) shows time evolution of the squared cross coherence between an on-vessel

magnetic probe and a chord of the ECE array at $r_{\text{eff}} \sim 0.15$ m as the representative

dynamics of the MHD mode. The coherent fluctuation mode first appears at $t_0 \sim 5.7$ s

and $f \sim 4.5$ kHz whose frequency chirps down stepwise as time progresses. Finally, the mode frequency becomes $f \sim 1$ kHz and disappears at $t \sim 5.9$ s. By performing the poloidal and toroidal mode structure analysis with the magnetic probe arrays, the mode number is determined to be $m/n = 2/1$, where m and n are the poloidal and toroidal mode numbers. The squared cross coherence γ^2 and the cross phase α are calculated at the various radial position of the ECE measurement with respect to the magnetic probe yielding the three-dimensional variables $\gamma^2(t, r_{\text{eff}}, f)$ and $\alpha(t, r_{\text{eff}}, f)$. From Fig. 2 (a), the time evolution of the mode peak frequency is defined as $f_{\text{peak}}(t)$. Taking values at $f = f_{\text{peak}}(t)$ from $\gamma^2(t, r_{\text{eff}}, f)$ and $\alpha(t, r_{\text{eff}}, f)$ provides the evolution of the mode radial structure, as shown in Figs. 2 (b) and (c). For the sake of visual clarity, the cross phase is only plotted in the case that the squared cross coherence is high enough. As time progresses and the frequency decays, the mode radial structure expands gradually, finally reaching the peripheral region of $r_{\text{eff}} \sim 0.5$ m. As shown in the phase profile, the mode structure is identified as the double-odd-parity until $t \sim 5.84$ s, which has two different phase inversion radii, at $r_{\text{eff}} \sim 0.1$ m and at 0.25 m. Figure 2 (d) presents the time evolution of the relative electron temperature gradient profile with respect to the value at $t_0 = 5.7$ s, defined as $\delta[-\nabla T_{\text{e}}(t, r)] = -\nabla T_{\text{e}}(t, r) + \nabla T_{\text{e}}(t_0, r)$. When the mode appears at $t_0 = 5.7$ s, the electron temperature gradient begins to decay at the two different phase inversion radii, $r_{\text{eff}} \sim 0.1$ m and 0.25 m, which are indicated by two arrows. These two flattening regions broaden as the mode evolves, and are connected to each other at $t \sim 5.81$ s, at which the sharp reduction of the central electron temperature

is observed. Interestingly, the outer phase inversion radius approaches toward the inner inversion radius after the central electron temperature collapse, at $t \sim 5.81$ s, and they are connected to each other at $t \sim 5.85$ s. This evolution makes the mode even-parity. After $t \sim 5.81$ s, the central electron temperature increases again while the mode exists.

In order to quantitatively discuss the dynamics of the mode and the electron temperature profile, time averaged cross coherence analysis is performed. Figures 3 rows (a) to (c) show the imaginary part of the cross spectrum that corresponds to the mode eigen function, the squared cross coherence, and the cross phase, respectively. The time averaging is performed in $5.72 < t < 5.75$ s (first column), $5.75 < t < 5.82$ s (second column), $5.82 < t < 5.84$ s (third column), and $5.86 < t < 5.90$ s (fourth column). Slices of the squared cross coherence and the cross phase at the peak frequency are shown in Fig. 3 row (d). Here, the mode width w_{mode} is defined as the maximum radial range that has the squared cross coherence larger than 0.5. The evolution of the electron temperature profiles are shown in Fig. 3 row (e) with those before the profile collapse occurs plotted by the dashed curves (first column of Fig.3). When the mode appears at the frequency of ~ 4.5 kHz, the mode width w_{mode} is ~ 0.23 m and the phase inversion width w_{inv}, i.e., the radial width between two phase inversion radii, is ~ 0.18 m. No clear flattening is seen in the electron temperature profile. As time progresses and the mode frequency decays down to ~ 3 kHz (second column of Fig.3), the mode width broadens while the phase inversion width shrinks. The flattened electron temperature profile seems to appear in $0.1 < r_{\mathrm{eff}} < 0.2$ m. In the next stage of the mode evolution (third

column of Fig.3), the mode frequency becomes ~ 1.5 kHz and further expansion of the mode width and further shrinking of the phase inversion width are observed. This stage corresponds to the time period shortly after the sharp central electron temperature decay at $t \sim 5.81$ s in Fig. 1 (c), so that a wide flattening region arises in $0.1 < r_{\mathrm{eff}} < 0.3$ m. In the last stage before the mode disappears (fourth column of Fig.3), the mode becomes the even-parity having no phase inversion layer. Even though the mode itself still exists, the electron temperature profile recovers comparable to that before the mode is driven.

Figure 4 shows how the mode width w_{mode} and phase inversion width $w_{\mathrm{inv.}}$ depend on the frequency. As the frequency decreases stepwise, w_{mode} increases while $w_{\mathrm{inv.}}$ decreases both approximately linearly. In the last stage, $w_{\mathrm{inv.}}$ becomes zero and w_{mode} saturates at ~ 0.37 m.

By use of the obtained mode properties, i.e., the poloidal mode number $m = 2$, the mode amplitude $A(r_{\mathrm{eff}})$, and the radial phase structure $\Phi(r_{\mathrm{eff}})$, the eigen function of the mode can be reconstructed as $\Psi(r_{\mathrm{eff}}, \theta) = A(r_{\mathrm{eff}}) \cos[-m\theta - \Phi(r_{\mathrm{eff}})]$. Figure 5 shows the time evolution of the reconstructed mode structure. As the mode evolves, the mode radial width expands and the phase inversion layer shrinks. In the final stage of the evolution, the phase inversion layer disappears and the mode parity becomes even.

2.3. Electron cyclotron current drive direction scan experiment

In order to investigate the impact of the ECCD on the mode appearance, we performed the ECCD scan experiment on the discharge scenario described in Fig. 1. The

Table 1. Relation between the ECCD directions and the mode appearance. Number of injected beams in each direction is shown in the parentheses.

Shot number	$\bar{n}_e$ [10^{19} m^{-3}]	co-ECCD [MW]	counter-ECCD [MW]	Mode appearance
150672	1.3	2.3 (3)	0 (0)	Yes
150673	1.3	1.5 (2)	0.8 (1)	Yes
150674	1.3	0.8 (1)	1.5 (2)	No
150676	1.3	0 (0)	2.3 (3)	No

ECCD from three launchers is injected to the base discharge with the beam switching. Combinations of the injection directions are scanned in the shot-to-shot manner. Table 1 shows the shot status regarding the ECCD direction and the mode appearance. When the number of the co-injected ECCDs surpasses that of the counter-injected ECCDs, the mode appears and the central electron temperature collapse occurs after the beam switching.

It is worthwhile to compare the rotational transform profile in these discharges measured by the motional Stark effect (MSE) spectroscopy [15] with an advanced analysis technique [18]. In the MSE spectroscopy system, the polarization angle of the probe beam emission is measured, from which the local magnetic pitch angle is evaluated. Change of the rotational transform from its vacuum value is estimated by the relative polarization angle from the reference shot, $\delta\gamma_{\mathrm{pol}}$. Here, the reference shot is produced by injecting the balanced co- and counter-NBs and by keeping the density as low as possible for minimizing a net plasma current. The plasma current profile in the

shot of interest that is consistent with $\delta\gamma_{\mathrm{pol}}$ is then chosen from a set of predetermined plasma current profiles. The radial profile of the relative polarization angle $\delta\gamma_{\mathrm{pol}}$ in #150672 is plotted in Fig. 6 as an example. Symbols show measured $\delta\gamma_{\mathrm{pol}}$ and curves represent the polarization angles derived from the chosen current profiles. As time progresses, the polarization angle increases, which corresponds to increasing $\iota/2\pi$ in time.

Figure 7 shows the time evolutions of the rotational transform profiles $\iota/2\pi$ derived from the relative polarization angle profiles measured by the MSE technique in each discharge. A quantitative discussion regarding the MHD mode onset and $\iota/2\pi$ profile shape evolution is still challenging due to poor temporal resolution and relatively large uncertainty in the core region, therefore we abandon to identify the magnetic shear reversal. Nevertheless, a clear qualitative difference in $\iota/2\pi$ profile evolution between the co-ECCD dominant cases and the counter-ECCD dominant cases is seen. In the cases of #150672 and #150673, the central $\iota/2\pi$ increases in time that makes the profile flattened or reversed near the rational surface of $\iota/2\pi = 1/2$. The transient beam switching from the co-NB to the counter-NB tends to increase the core $\iota/2\pi$ and to decrease the edge $\iota/2\pi$ [14, 15]. The co-injected ECCDs that have a more localized deposition in the core likely assist the increment of $\iota/2\pi$ in the core. In the other cases, $\iota/2\pi$ stays almost unchanged. The counter-injected ECCDs seem to compensate the NB-driven current change, which help to prevent the MHD mode appearance. Therefore, the counter-ECCD is an effective control tool for this MHD mode induced electron temperature

profile collapse.

3. Discussion

Now we discuss the origin of the double-odd-parity mode. One possibility is the resistive

interchange mode, which can be unstable in the magnetic hill of the LHD inward shifted

magnetic axis configuration. The beam switching operation can trigger such a mode

by weakening the magnetic shear or making a reversed shear iota profile with two

rational surfaces. Although the eigen mode function of the resistive interchange mode

is considered to be the even-parity in general, it is predicted that the odd-parity is also

possible as the secondary eigen mode function [19]. Since the radial mode structure

observed is the double-odd-parity possibly having a tearing mode nature, the double

tearing mode driven by external current drive would be another candidate. As discussed

in [20], even in heliotron devices a tearing mode can be excited in the reversed iota

profile. However, the mode is predicted to be solely at the inner $\iota/2\pi = 0.5$ surface,

while the observation shows a much wider mode structure being inconsistent with the

theoretical model [20]. The tearing mode excitation was observed in W7-AS stellarator

by an intense ohmic current [8].

In the later phase of the mode evolution the mode parity transits to the even

parity, implying a different driving mechanism of the mode. Since the central iota is

continuously increasing and the $\iota/2\pi = 0.5$ rational surface is considered to eventually

disappear keeping the magnetic shear very small. This situation resembles to the

condition in which the 'infernal' mode emerges [21]. One of the keys for the mode identification is the accurate rotational transform profile measurement in the core with a high time resolution, which is still very challenging with the current MSE system in LHD.

4. Summary

In this paper, we reported new results of a beam switching experiment aiming at a reversed magnetic shear profile formation for the study of an MHD mode induced profile collapse event. A transient MHD mode whose oscillation frequency chirps down was observed. The electron temperature profile collapse was induced by the mode activity, leading to the flattening of the central electron temperature profile. The radial mode structure was the double-odd-parity at the beginning, but it transited to the even-parity in its final stage. The central electron temperature profile recovered after the radial mode structure changes to the even-parity, even though the mode itself did not disappear.

References

[1] Y Koide, M Kikuchi, M Mori, S Tsuji, S Ishida, N Asakura, Y Kamada, T Nishitani, Y Kawano, T Hatae, *et al* 1994 *Phys. Rev. Lett.* **72** 3662

[2] E Joffrin, CD Challis, GD Conway, X Garbet, A Gude, S Günter, NC Hawkes, TC Hender, DF Howell, GTA Huysmans, *et al* 2003 *Nucl. Fusion* **43** 1167

[3] T Estrada, D López-Bruna, A Alonso, E Ascasíbar, A Baciero, A Cappa, F Castejón, A Fernández, J Herranz, C Hidalgo, *et al* 2006 *Fusion Sci. Tech.* **50** 127–135

[4] K A Razumova, V V Alikaev, A A Borschegovskii, V V Chistyakov, M M Dremin, A V Gorshkov, A Ya Kislov, D A Kislov, S V Krylov, S E Lysenko, *et al* 2000 *Plasma Phys. Control. Fusion* **42** 973

[5] H Takahashi, K Nagaoka, K Mukai, M Yokoyama, S Murakami, S Ohdachi, T Bando, Y Narushima, H Nakano, M Osakabe, *et al* 2018 *Nucl. Fusion* **58** 106028

[6] J Mailloux, B Alper, Y Baranov, A Becoulet, A Cardinali, C Castaldo, R Cesario, G Conway, CD Challis, F Crisanti, *et al* 2002 *Phys. Plasmas* **9** 2156–2164

[7] Z Chang, W Park, ED Fredrickson, SH Batha, MG Bell, R Bell, RV Budny, CE Bush, A Janos, FM Levinton, *et al* 1996 *Phys. Rev. Lett.* **77** 3553

[8] A Weller, J Geiger, A Werner, MC Zarnstorff, C Nührenberg, E Sallander, J Baldzuhn, R Brakel, R Burhenn, A Dinklage, *et al* 2003 *Plasma Phys. Control. Fusion* **45** A285

[9] S Sakakibara, KY Watanabe, S Ohdachi, Y Narushima, K Toi, K Tanaka, K Narihara, K Ida, T Tokuzawa, K Kawahata, *et al* 2010 *Fusion Sci. Tech.* **58** 176–185

[10] Y Takemura, S Sakakibara, Y Narushima, M Okamoto, KY Watanabe, Y Suzuki, S Ohdachi, K Ida, M Yoshinuma, K Tanaka, *et al* 2012 *Nucl. Fusion* **52** 102001

[11] Y Takemura, KY Watanabe, S Sakakibara, S Ohdachi, Y Narushima, K Ida, M Yoshinuma, H Tsuchiya, T Tokuzawa, I Yamada, *et al* 2019 *Nucl. Fusion* **59** 066036

[12] S Günter, S Schade, M Maraschek, SD Pinches, E Strumberger, R Wolf, Q Yu, and

ASDEX Upgrade Team 2000 *Nucl. Fusion* **40** 1541

[13] DA Humphreys, JR Ferron, RJ La Haye, TC Luce, CC Petty, R Prater, and AS Welander 2006 *Phys. Plasmas* **13** 056113

[14] K Ida, S Inagaki, M Yoshinuma, Y Narushima, K Itoh, T Kobuchi, KY Watanabe, H Funaba, S Sakakibara, T Morisaki, *et al* 2008 *Phys. Rev. Lett.* **100** 045003

[15] K Ida, M Yoshinuma, C Suzuki, T Kobuchi, KY Watanabe, and LHD Experiment Group 2010 *Fusion Sci. Tech.* **58** 383–393

[16] K Ida, S Inagaki, Y Suzuki, S Sakakibara, T Kobayashi, K Itoh, H Tsuchiya, C Suzuki, M Yoshinuma, Y Narushima, *et al* 2013 *New J. Phys.* **15** 013061

[17] C Suzuki, K Ida, Y Suzuki, M Yoshida, M Emoto, and M Yokoyama 2012 *Plasma Phys. Control. Fusion* **55** 014016

[18] TJ Dobbins, K Ida, C Suzuki, M Yoshinuma, T Kobayashi, Y Suzuki, and M Yoshida 2017 *Rev. Sci. Instrum.* **88** 093518

[19] R Ueda, KY Watanabe, Y Matsumoto, M Itagaki, M Sato, and S Oikawa 2014 *Phys. Plasmas* **21** 052502

[20] K Ichiguchi 2002 *J. Plasma Fusion Res. SERIES* **5** 491–494

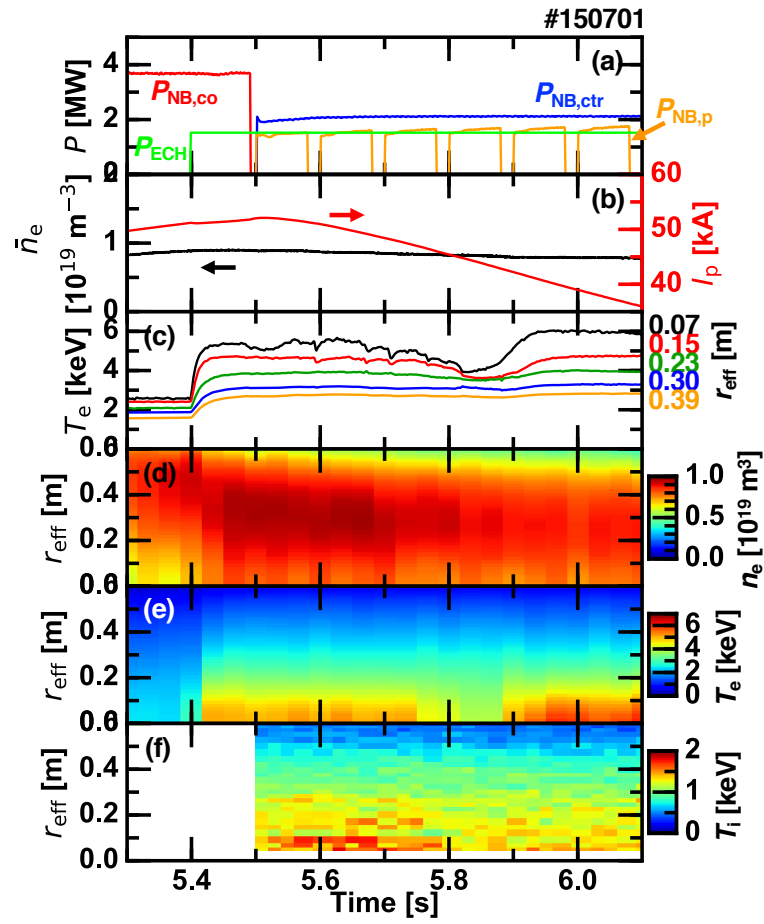[21] J Manickam, N Pomphrey, and AMM Todd 1987 *Nucl. Fusion* **27** 1461

Figure 1. Time evolutions of (a) heating power, (b) line averaged density and plasma current, (c) electron temperature, (d) electron density profile, (e) electron temperature profile, and (f) ion temperature profile.
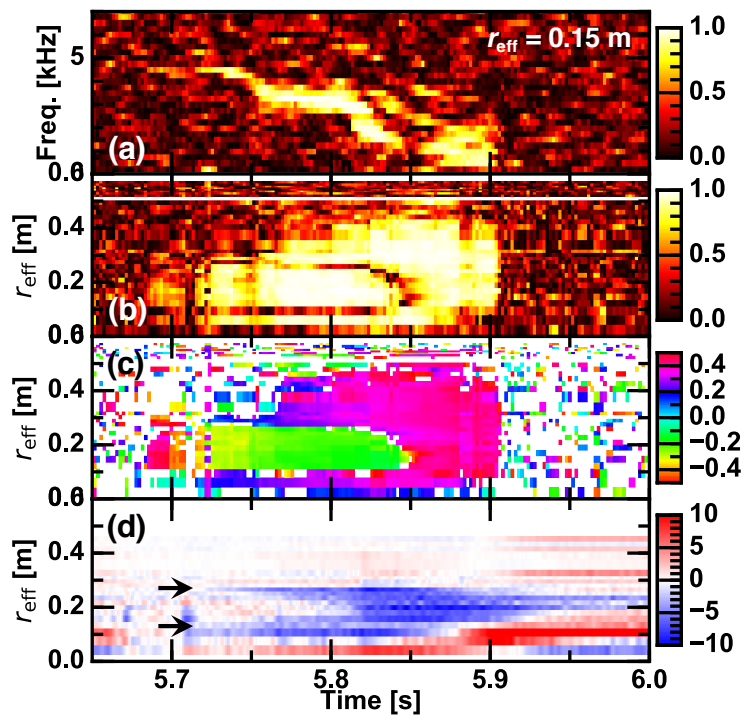
Figure 2. Time evolutions of (a) squared cross coherence spectrum between the ECE signal and the magnetic probe signal, (b) squared cross coherence profile, (c) cross phase profile, and (d) electron temperature gradient profile.
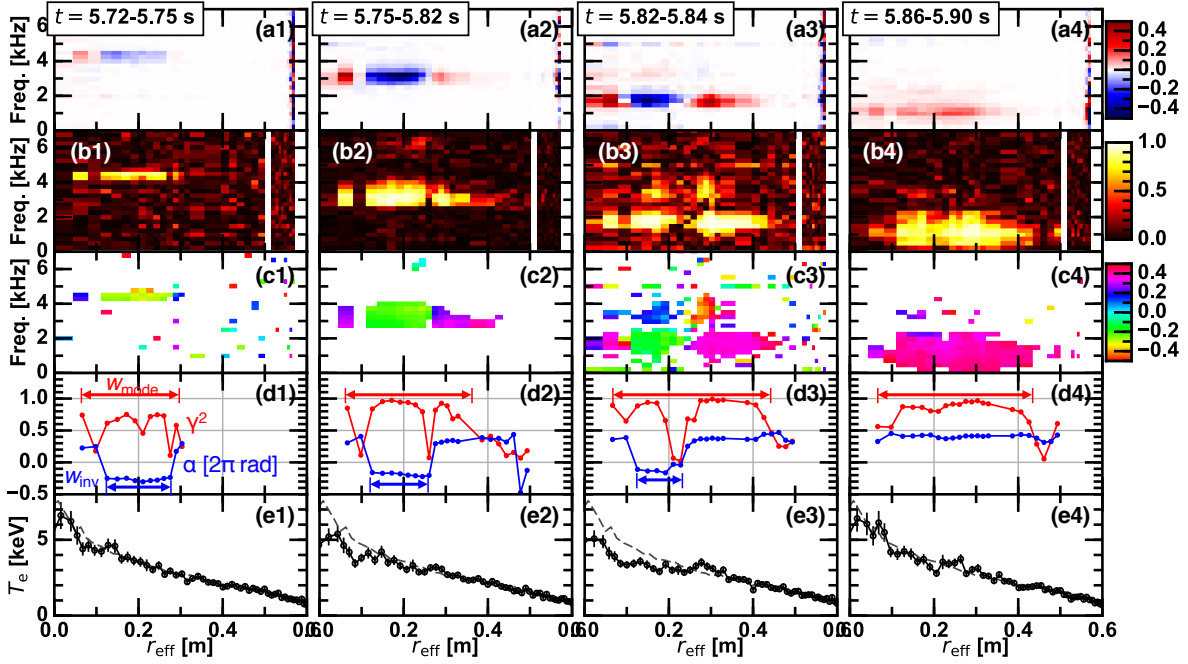
Figure 3. Radial profiles of various MHD mode related parameters in $t = 5.72 - 5.75$ s (first column), $t = 5.75 - 5.82$ s (second column), $t = 5.82 - 5.84$ s (third column), and $t = 5.86 - 5.90$ s (fourth column): (a) imaginary part of the cross spectrum density, (b) squared cross coherence, (c) cross phase, (d) slices of the squared cross coherence and the cross phase at the peak frequency, and (d) electron temperature profile. Dashed curves in (e) show the electron temperature profile before the profile collapse occurs.
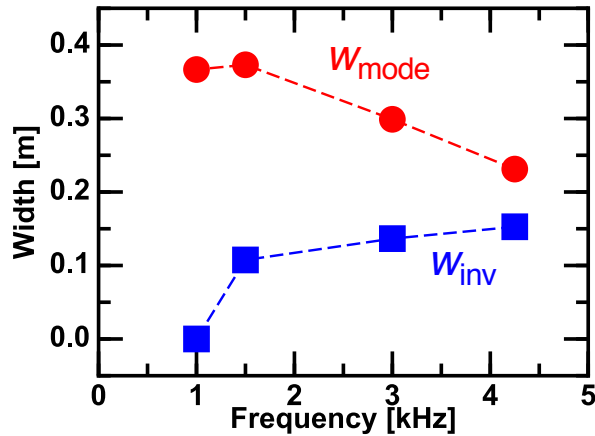
Figure 4. Mode width and phase inversion layer width plotted against the mode frequency.
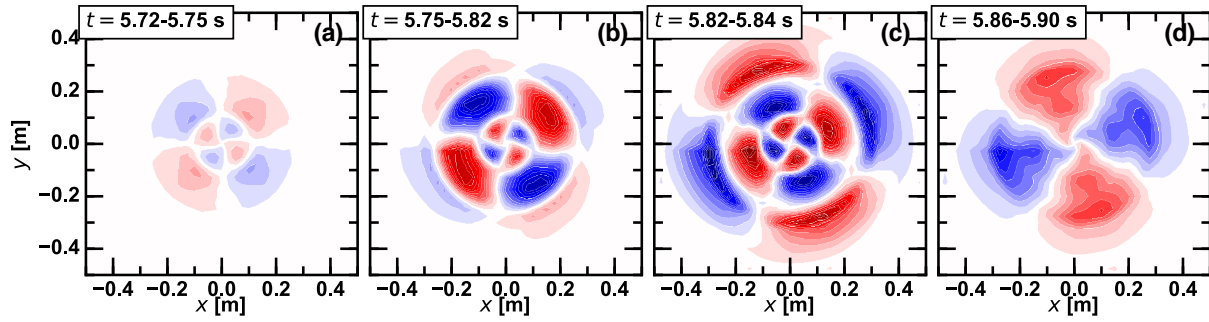
Figure 5. Reconstructed mode structure in the arbitrary poloidal cross section in (a) $t = 5.72 - 5.75$ s, (b) $t = 5.75 - 5.82$ s, (c) $t = 5.82 - 5.84$ s, and (d) $t = 5.86 - 5.90$ s.
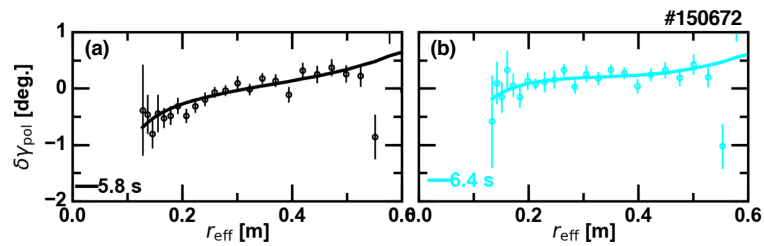

Figure 6. Radial profiles of the relative polarization angle from the reference shot at (a) $t = 5.8$ s and (b) $t = 6.4$ s for $\#$ 150672. Symbols show the measured data point and curves represent the polarization angle profiles derived from the chosen current profiles.
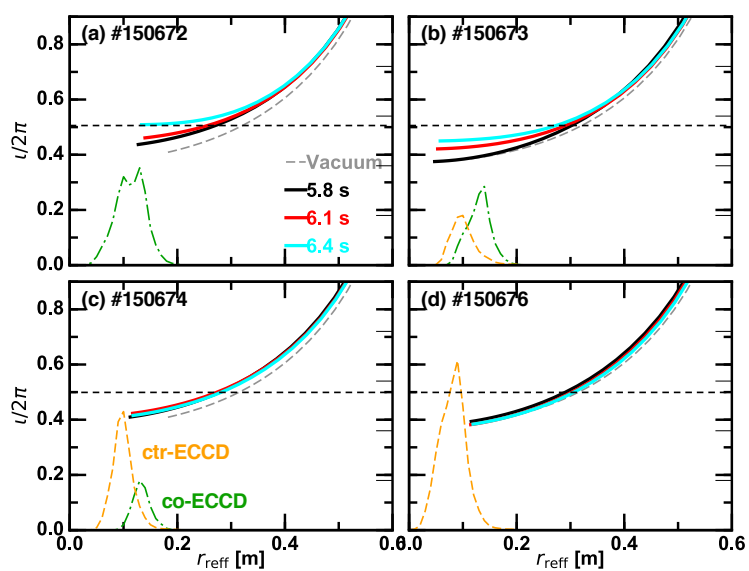
Figure 7. Radial profiles of the rotational transform and the ECCD deposition in (a) # 150672, (b) # 150673, (c) # 150674, and (d) # 150676.